




Modeling of Single Porous Char Particle Gasification in Supercritical Water

Chao Fan¹ · Qiuyang Zhao¹ · Jialing Xu¹ · Hui Jin¹ 

Received: 19 September 2020 / Accepted: 27 September 2021 / Published online: 2 November 2021
© The Author(s), under exclusive licence to Springer Nature B.V. 2021

Abstract

A deep understanding of the gasification behavior of porous char particle is the premise of the reactor-scale modeling, but there are few studies on the gasification characteristics in supercritical water. Thus, a numerical model for porous char particle gasification in supercritical water was developed in this work, and the effects of particle size, inflow temperature and inflow velocity were studied. Simulation results showed that gasification of the small particle of 0.1 mm lay in zone I regime where the particle radius kept unchanged due to uniform reactions inside the particle and the effectiveness factor increased rapidly after the gasification began due to easy accessibility of supercritical water into the particle. The gasification of the large particle of 1 mm showed typical characteristics in zone II regime that the particle began to shrink at a certain conversion degree, and smaller effectiveness factor was observed due to larger supercritical water concentration gradient inside the particle. As the increase of temperature and particle size, ambient fluid became difficult to flow through the unreacted core, and the Stefan flow was observed to obviously modify the hydrodynamic boundary layer at low Reynolds number. Besides, it is unreasonable to assume isothermal particle for gasification with large particle and high temperature because of the significantly overestimated particle consumption rate.

Article Highlights

1. Numerical simulation was conducted on a porous char particle in supercritical water with structural evolution;
2. Gasification of 0.1 mm and 1 mm particles, respectively, lay in kinetics and pore diffusion-controlled regimes;
3. Stefan flow modified the hydrodynamic boundary layer obviously at low Reynolds number.

✉ Hui Jin
jinhui@mail.xjtu.edu.cn

¹ State Key Laboratory of Multiphase Flow in Power Engineering (SKLMF), Xi'an Jiaotong University, 28 Xianning West Road, Xi'an 710049, Shaanxi, China

Keywords Supercritical water gasification · Porous char · Numerical modeling · Effectiveness factor · Stefan flow

1 Introduction

Coal accounts for the most proportion in the energy consumption of China due to its good availability and low cost, and this situation will not be changed in the near future (Jiang et al. 2019). Unfortunately, the conventional coal utilization is one of the main sources of environmental concern because of its high emission of greenhouse gas, nitrogen and sulfur oxides and dust (Yuan et al. 2018). For these reasons, the development of clean coal technologies is important and practical. Owing to the excellent properties of supercritical water (SCW) such as high reactivity, high diffusivity and high solubility for organic matters, coal can be converted into hydrogen-rich syngas in SCW under milder temperature conditions compared with traditional gasification processes and the pollutant emission can be inhibited from the source (Guo and Jin 2013; Li et al. 2022; Zhao et al. 2021). Thus, the technology of supercritical water gasification (SCWG) is believed to be an efficient, clean and promising way for coal utilization.

Char particle consumption is the key step in the coal gasification/combustion process because of its significantly lower rate than pyrolysis and the mass production of gas products; thus, special attention is usually paid to this process to reveal the detailed conversion characteristics. The porous structure of char particle evolves in the conversion process, which directly affects the species transport along the pores and reactions on the pore surface. Therefore, char particle gasification is a complex coupling process of species transport, heat transfer, chemical reaction and structural evolution. Extensive research has been carried out to study the porous char conversion at particle scale, and numerical simulation is an effective and necessary method to reveal the conversion details that are difficult to obtain experimentally. The porous char was treated as one-dimensional structure for simplification in some studies. Sadhukhan et al. (2010b) developed a model in-house to study the combustion characteristics of a single porous char particle with high ash content, and the effects of temperature, pressure and particle size were discussed. For comprehensive predication of the gasification/combustion process, the model by Singer and Ghoniem (2013) accounted for annealing, particle size reduction and ash adherence simultaneously. Particularly, the adaptive random pore model was adopted to allow different pore to grow at different rates. Despite the low computational cost, the one-dimensional models cannot consider the convective effects which might not be ignored at high Reynolds number (Fan et al. 2020). Beckmann et al. (2017) simulated the gasification process of a 5.2-mm char particle in CO₂ at a particle Reynolds number of 140, using a two-dimensional axis-symmetric model. The calculated results fitted the experimental data well, and detailed structural evolution, temperature and species distribution characteristics were revealed. Tufano et al. (2019) also presented a two-dimensional model for a single particle, in which heating, ignition, volatile combustion and char conversion were all considered in convective gas environments. In addition, some three-dimensional models based on the true char porous structure were developed (Fong et al. 2018; Numazawa et al. 2020). True pore structure can be resolved in these models when compared with the porous media based on effective-continuum assumption. However, the pore-resolved direct numerical simulation on the porous particle required significantly higher computing capability and the energy equation was even neglected in Numazawa's model to reduce the computational load. Based on the

extensive particle-scale studies, essential and useful information can be obtained for developing accurate particle conversion sub-models in reactor-scale modeling and simulation (Zhang et al. 2016).

However, the previous studies all served the traditional combustion and gasification processes, and the SCWG process was particularly poorly studied. Although some general laws for particle conversion can be concluded from the existing work, the unique physical properties of SCW must be reconsidered for in-depth understanding of char particle gasification characteristics in SCWG process. For example, the reactant concentration at high pressure above 22.1 MPa is one to two orders of magnitude higher than that in conventional combustion/gasification environment, thus avoiding the restriction of mass transport on particle gasification. Besides, the characteristics of radiation and diffusion are also affected. Thus, this paper aims to develop a specialized model with the unique properties (density, specific heat, thermal conductivity and viscosity) of SCW implanted. Relevant parameters of radiation (Ren et al. 2018), species diffusion (Zhao and Jin 2020) and reaction kinetics (Su et al. 2016), which were obtained in our group and specifically used for SCW conditions, are adopted in the model. A CFD-based 2D transient numerical model coupling flow, heat transfer, species diffusion and chemical reactions is developed to reveal the gasification details of a single porous char particle in SCW, and the effects of inflow temperature, velocity and particle size are studied.

2 Modeling

2.1 Model Description

In the developed model in this work, a single spherical porous char particle is placed at a fixed position in the flow field, with SCW flowing around it. The char particle is assumed to consist carbon only, and its initial porosity and specific surface area are, respectively, 0.3 and $10^6 \text{ m}^2 \cdot \text{m}^{-3}$. The computational domain is selected to be large enough compared to the char particle to avoid blockage effects, and its size is shown in Fig. 1. A two-dimensional axisymmetric model is used to describe the three-dimensional process, and the effect of gravity is therefore neglected.

The velocity-inlet and pressure-outlet boundary conditions are, respectively, specified for the inlet and outlet, and the adiabatic and slip wall boundary condition is used for the side wall to ensure the inflow velocity to be uniform over the inlet cross section. For all studied cases, the inflow temperature T_{in} varies from 873 to 1023 K and the inflow pressure

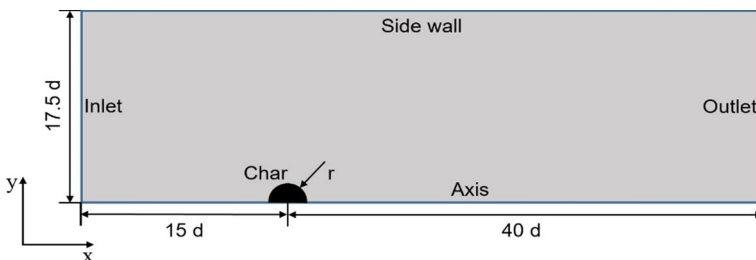


Fig. 1 Schematic diagram of the computational domain

is held at 25 MPa. The inflow velocity u_{in} is determined by the particle Reynolds number ranging from 0 to 100 and is defined as:

$$\text{Re} = \frac{\rho_{\text{in}} u_{\text{in}} d}{\mu_{\text{in}}} \quad (1)$$

where ρ_{in} and μ_{in} are, respectively, the density and molecular viscosity of inflow SCW and d is the particle diameter with a value of 0.1 or 1 mm for different cases. Specially, the physical properties (density, specific heat, thermal conductivity and viscosity) of SCW are calculated by IAPWS-IF97 (Wagner et al. 1997) and implanted in the model using piecewise polynomial functions of temperature.

For the initial conditions, the porous char is filled with CO_2 rather than SCW to avoid the unrealistic high initial reaction rate and to simulate the process of reactant diffusion into the particle. The initial temperature in the whole computational domain is set to be equal to the inflow temperature.

2.2 Governing Equations

2.2.1 Governing Equations in Fluid Region

The general transient mass, momentum and energy conservation equations and species transport equation are solved in the fluid region surrounding the particle. Specifically, the mass and momentum conservation equations take the form:

$$\frac{\partial \rho}{\partial t} + \nabla \cdot (\rho u) = 0 \quad (2)$$

$$\frac{\partial(\rho u)}{\partial t} + \nabla \cdot (\rho u u) = -\nabla P + \nabla \cdot (\tau) \quad (3)$$

where ρ , t , u , P stand for the fluid density, time, flow velocity and static pressure, respectively. The stress tensor τ is given by

$$\tau = \mu \left[(\nabla u + (\nabla u)^T) - \frac{2}{3} \nabla \cdot u I \right] \quad (4)$$

with μ as the molecular viscosity and I as the unit tensor.

The energy conservation equation and species transport equation write as:

$$\frac{\partial(\rho h)}{\partial t} + \nabla \cdot (\rho u h) = \nabla \cdot (\lambda \nabla T - q_r) - \sum_i \frac{h_i^0}{M_i} R_i \quad (5)$$

$$\frac{\partial(\rho Y_i)}{\partial t} + \nabla \cdot (\rho u Y_i) = \nabla \cdot (\rho D_{i,m} \nabla Y_i) + R_i \quad (6)$$

with h as the enthalpy and λ as the thermal conductivity. The P-1 radiation model is adopted to describe the gas-gas radiation and q_r is the gas-phase radiation source. The radiation absorption coefficient in SCW environment is obtained from the reference (Ren et al. 2018). h_i^0 , M_i and R_i stand for the enthalpy of formation, molecular weight and net production rate, respectively, of species i . In the species transport equation, Y_i denotes the mass

fraction of species i , and $D_{i,m}$ is the mass diffusion coefficient of species i in the mixture which is derived from the reference (Zhao and Jin 2020).

2.2.2 Governing Equations in Porous Particle Region

In the porous particle, both the effects of porosity and chemical reactions should be considered. The continuity equation takes the following form:

$$\frac{\partial(\epsilon\rho)}{\partial t} + \nabla \cdot (\epsilon\rho u) = S_m \tag{7}$$

with ϵ as the porosity, and S_m is mass source caused by carbon consumption.

The momentum conservation equation is written as:

$$\frac{\partial(\epsilon\rho u)}{\partial t} + \nabla \cdot (\epsilon\rho uu) = -\epsilon\nabla P + \nabla \cdot (\epsilon\tau) - \frac{\epsilon^2\mu}{K}u \tag{8}$$

where the third term on the right-hand side is the viscous loss term accounting for the fluid–solid interaction. K is the permeability given by the Blake–Kozeny equation (Ergun 1952):

$$K = \frac{d_p^2\epsilon^3}{150 \cdot (1 - \epsilon)^2} \tag{9}$$

where d_p is the average pore diameter and can be calculated with (Szekely 2012):

$$d_p = \frac{4\epsilon}{S_v} \tag{10}$$

where S_v is the surface area per volume and correlates with the carbon conversion X_c through the random pore model (Bhatia and Perlmutter 1980):

$$S_v = S_{v,0}(1 - X_c)\sqrt{1 - \psi \ln(1 - X_c)} \tag{11}$$

where $S_{v,0}$ is the initial SSA and ψ is the pore structural parameter with a value of 4 in this work. The carbon conversion X_c is defined as:

$$X_c = \frac{\epsilon - \epsilon_0}{1 - \epsilon_0} \tag{12}$$

with ϵ_0 as the initial porosity.

The energy conservation equation and species transport equation, respectively, are written as:

$$\frac{\partial(\epsilon\rho h + (1 - \epsilon)\rho_s h_s)}{\partial t} + \nabla \cdot (\epsilon\rho uh) = \nabla \cdot (\lambda_{\text{eff}}\nabla T) - \sum_i \frac{h_i^0}{M_i}R_i \tag{13}$$

$$\frac{\partial(\epsilon\rho Y_i)}{\partial t} + \nabla \cdot (\epsilon\rho u Y_i) = \nabla \cdot (\rho D_{i,m,\text{eff}}\nabla Y_i) + R_i \tag{14}$$

where the subscript s represents the solid char, and the carbon true density is assumed to be $2000 \text{ kg}\cdot\text{m}^{-3}$ here. λ_{eff} is the effective thermal conductivity defined as:

$$\lambda_{\text{eff}} = \varepsilon \lambda + (1 - \varepsilon) \lambda_s \quad (15)$$

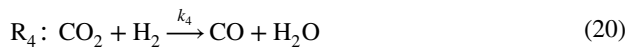
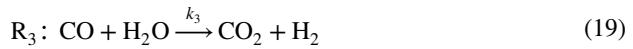
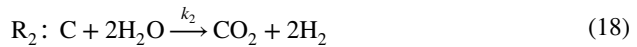
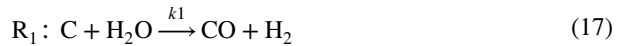
In the porous particle, the diffusion is affected by the pore structure, and the effective mass diffusion coefficient for species i can be calculated by (Szekely 2012):

$$D_{i,m,\text{eff}} = \frac{\varepsilon}{\gamma} D_{i,m} \quad (16)$$

where γ is the tortuosity which is assumed to be the reciprocal of porosity as $\gamma = \varepsilon^{-1}$. Knudsen diffusion inside the porous particle was ignored because the molecule movement was restricted at such a high pressure and the molecule average free path was sufficiently small compared to the pore size.

2.3 Reaction Kinetics

Heterogeneous reactions R_1 , R_2 in porous char and homogeneous reactions R_3 , R_4 in the whole computational domain are considered in this model, as seen below:



The reaction rate constant k_j is calculated using the Arrhenius equation:

$$k_j = A_j \exp\left(\frac{-E_{aj}}{RT}\right) \quad (21)$$

where A_j and E_{aj} are, respectively, the pre-exponential factor and activation energy for reaction R_j , and R is the universal gas constant. Kinetic parameters are based on Su's work (Su et al. 2016) as listed in Table 1.

The source terms R_i in the species transport equation and S_m in continuity equation can therefore be expressed as:

Table 1 Kinetic parameters and volumetric reaction rate

Reactions	Rate constants	$\ln A_j$	E_{aj} (kJ·mol ⁻¹)	Volumetric reaction rate R_j^v (mol·m ⁻³ ·s ⁻¹)
R_1	k_1	-8.1678	27.76	$k_1 C_{\text{H}_2\text{O}} S_V$
R_2	k_2	12.3465	176.64	$k_2 C_{\text{H}_2\text{O}} S_V$
R_3	k_3	7.2192	96.83	$k_3 C_{\text{CO}} C_{\text{H}_2\text{O}}$
R_4	k_4	11.2	133.06	$k_4 C_{\text{CO}_2} C_{\text{H}_2}$

$$R_i = \sum_j \vartheta_{i,j} M_i R_j^V \quad (22)$$

$$S_m = \sum_{j=1}^2 M_{\text{carbon}} R_j^V \quad (23)$$

where $\vartheta_{i,j}$ is the stoichiometric coefficient for species i in reaction R_j , and M_i is the molecular weight of species i .

2.4 Discretization and Numerical Consideration

The computational domain in Fig. 1 was discretized by the finite volume method, and the commercial software ICEM CFD was used to generate structured grids as seen in Fig. 2. According to the concept of representative elementary volume (REV), the grid size in the porous zone should be large enough compared to the pore size. Given the values of initial porosity and specific surface area of respective 0.3 and $10^6 \text{ m}^2 \text{ m}^{-3}$ in Sect. 2.1, the initial pore diameter can be calculated as $1.2 \text{ }\mu\text{m}$ using Eq. 10. To satisfy the above requirement, sufficiently sparse grids must be adopted, especially for the small particle of 0.1 mm . Even so, the pore size keeps increasing in the gasification process and will finally become larger than the grid size inevitably. Moreover, some important gasification details might be lost using too sparse grids. Thus, the above limitation was ignored in this work, and fine grids were used to capture the detailed information of temperature and species distribution inside the porous char particle. The commercial software ANSYS FLUENT 18.2 was used to solve the problem above. The coupled algorithm was used for pressure–velocity coupling, and convective terms in all equations were discretized using the second-order upwind scheme. An initial time step of 1 ms was chosen for each calculation, and the time step was increased gradually as the calculation tended to be stable.

It should be emphasized that the model validation with experimental results was not attempted in this work. Under the strictly sealed environment with high temperature and pressure, the traditional thermogravimetric method is invalid, and it is difficult to design experiments to obtain the real-time changes in temperature and mass of a single char particle in SCW. In the existing batch SCWG reactor in our lab (Jin et al. 2018), the slow heating and cooling make the data obtained inaccurate, and it is impractical to conduct experiments with a single particle. Fortunately, the validity of the basic modeling method in this

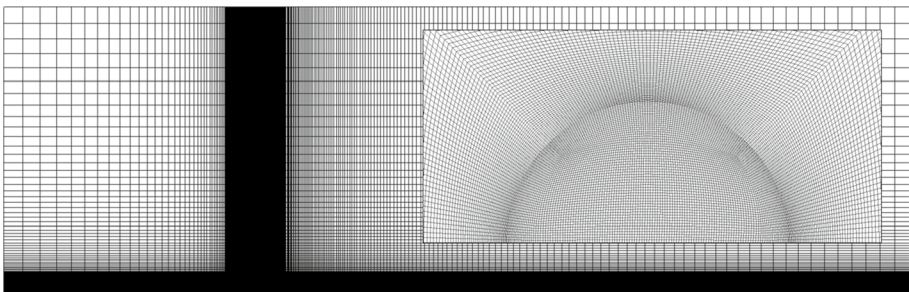


Fig. 2 Grid of the computational domain

study has been experimentally confirmed with conversion of millimeter-sized char particles under traditional conditions (Beckmann et al. 2017; Bhunia et al. 2017; Sadhukhan et al. 2010a), and these studies also provided valuable references for this paper. Here, we performed a particle-resolved simulation to further develop a sub-model of char particle gasification for reactor-scale modeling. The accuracy of the proposed sub-model will be verified by comparing simulation results and experimental results of the SCW fluidized bed gasifier in our laboratory (Fan et al. 2019).

3 Results and Discussion

Above all, the evolution of carbon conversion X_c with time is displayed in Fig. 3. The reactivity under different conditions was evaluated using the index $R_{0.5}$ ($0.5/t_{0.5}$, and $t_{0.5}$ is the gasification time when X_c reaches 0.5) (Senneca and Salatino 2002). As the temperature increased from 873 to 1023 K, $R_{0.5}$ increased from 0.165 to 1.294 s^{-1} and 0.018 to 0.052 s^{-1} for the small and large particles, respectively, because of enhanced gasification. It is well known that the porous char gasification shifts from kinetics controlled to diffusion-controlled regime with the increase of temperature and particle size. To investigate the effect of convection under different regimes, the inflow velocity was adjusted to obtain different Re for the small particle at 873 K and for the large particle at 1023 K, respectively. The kinetics-controlled regime usually represents a uniform distribution of temperature and species concentration inside the particle, so the promotion of convection on heat and mass transport was limited. As shown in Fig. 3a, $R_{0.5}$ increased just from 0.165 to 0.196 s^{-1} when Re increased from 0 to 100. By contrast, the effect of convection in diffusion-controlled regime was obvious. As shown in Fig. 3b, $R_{0.5}$ increased from 0.052 to 0.101 s^{-1} with the same increase of Re. The char gasification characteristics under different regimes will be further discussed in the following sections.

3.1 Species Distribution

Figure 4 shows the species mole fraction distribution inside the porous particle at the X_c of 0.5, and CO was not considered because of its low proportion in the produced gases. As

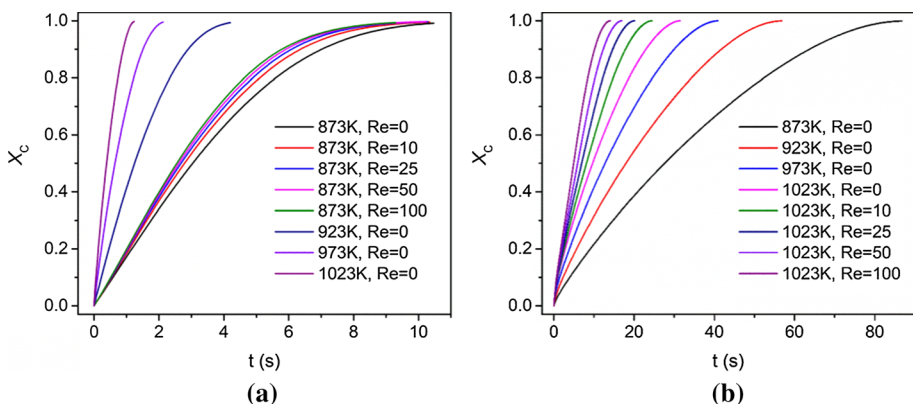


Fig. 3 Carbon conversion with time for particles of 0.1 mm (a) and 1 mm (b)

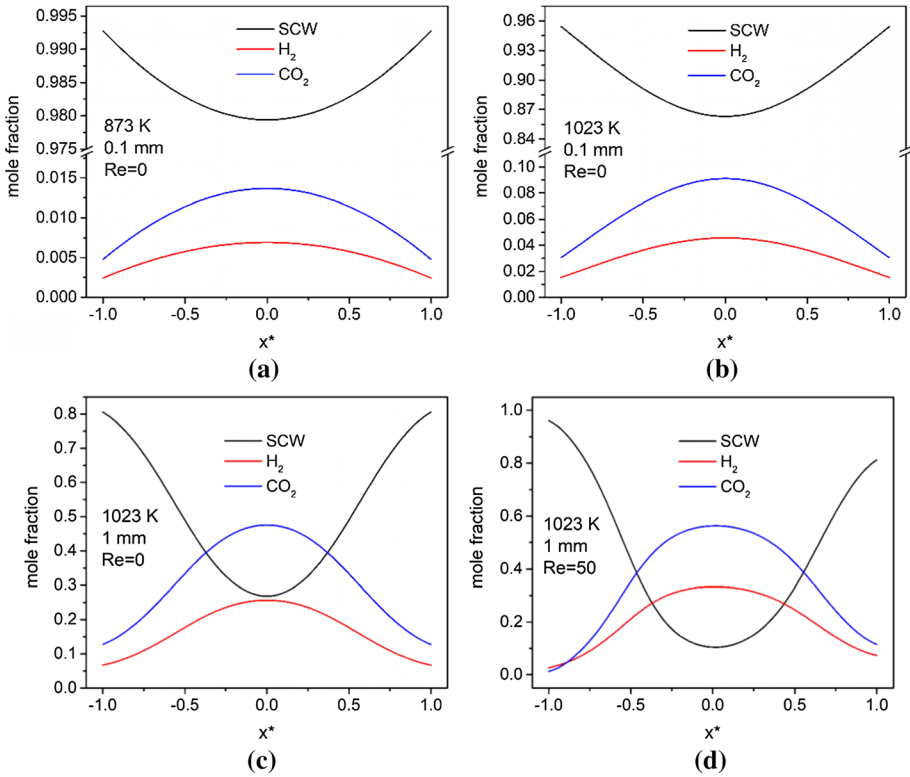


Fig. 4 Species mole fraction distribution along the x-axis at the X_c of 0.5 ($x^* = x/r_{p,0}$, x and $r_{p,0}$, respectively, represent the abscissa value and initial particle radius)

expected, the SCW concentration declined from the outside to the inside when it entered the particle, while the produced gases diffused outside of the particle with the opposite concentration gradients. For the case in Fig. 4a, the concentration of SCW inside the particle was much higher than that of the produced gases due to the slow gas production at a low temperature and the easy species diffusion inside a small particle. The mole fraction of CO₂ and H₂ was less than 0.015 even at the center of the particle. As the temperature rose to 1023 K, more gases were produced, but their concentrations were still obviously less than SCW concentration, as shown in Fig. 4b. With the particle size increasing, more SCW was further consumed when it entered deep into the particle and it was more difficult for the produced gases to diffuse to the outside of the particle, as shown in Fig. 4c. As a result, the CO₂ and H₂ concentration significantly increased, and the CO₂ mole fraction of 0.48 was even higher than the SCW mole fraction of 0.27 at the particle center. The effect of convection is shown in Fig. 4d. After the external flow was imposed, an obviously asymmetrical species concentration distribution was observed. On the upwind side, the SCW mole fraction at Re of 50 was higher than that at Re of 0 due to mass transfer enhancement by convection. Meanwhile, the heat transfer was also promoted which led to a higher particle temperature and faster SCW consumption. Thus, as the position got deeper into the particle, the SCW mole fraction at Re of 50 decreased rapidly and became lower than that at Re of 0, with a minimum value of 0.1 at the particle center. Besides, it was noticed that the

mole fraction of CO_2 was almost always higher than that of H_2 inside the particle, though more H_2 was produced than CO_2 according to reactions R_{1-4} , and this can be explained by higher molecular diffusion coefficient of H_2 .

3.2 Structural Evolution

Char particle radius and apparent density are usually important real-time variables to be acquired in the reactor-scale simulation of gasification/combustion process, and the development of char particle conversion sub-models depends closely on the particle conversion mode (Haugen et al. 2015; Kaushal et al. 2010; Rabaçal et al. 2018). In zone I conversion regime, the particle reacts uniformly throughout its volume, where the particle size keeps unchanged and the apparent density varies proportionally to the particle conversion degree. In contrast, in zone III conversion regime, the reaction primarily occurs at particle periphery, where the particle radius varies to the one-third power of the particle conversion degree and the apparent density keeps constant. Between the two extreme situations is the zone II regime where both radius and apparent density change in the conversion process, and the existence of species and apparent density gradients inside the particle makes the conversion mechanism complicated and difficult to describe.

Here, we assume the particle shrinks when the local carbon conversion in the outermost layer exceeds 0.99 and the equivalent spherical radius (radius of a sphere of equivalent volume) is adopted for irregular spheres under convective conditions. The final evolution of particle radius and apparent density with X_c is displayed in Figs. 5 and 6, respectively. For the char particle of 0.1 mm, the particle radius remained unchanged until it sharply decreased to 0 at the end of the gasification, while the apparent density decreased linearly with the carbon conversion. Based on the above discussion, the small char particle gasification can be thought to lie in zone I regime. Therefore, the particle radius can be assumed to be constant for simulation of SCWG process in a fluidized bed reactor where the particle size usually does not exceed 0.1 mm. For gasification of large char particle of 1 mm in the zone II regime, it was observed that the particle radius began to decrease at a certain X_c and the apparent density no longer evolved linearly with X_c . In addition, when the temperature and Re increased, the gasification was promoted and the SCW had no time to diffuse deeper into the particle, causing the reactions to occur mainly in the outer region and the

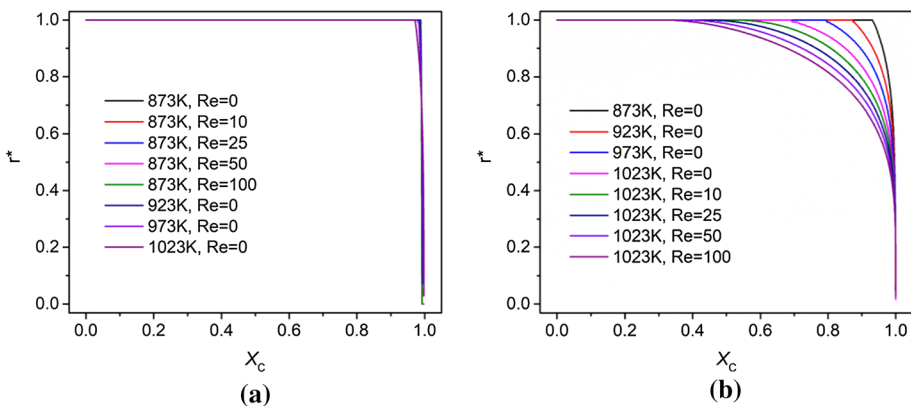


Fig. 5 Particle radius evolution with X_c for particles of 0.1 mm (a) and 1 mm (b) ($r^* = r_p/r_{p,0}$)

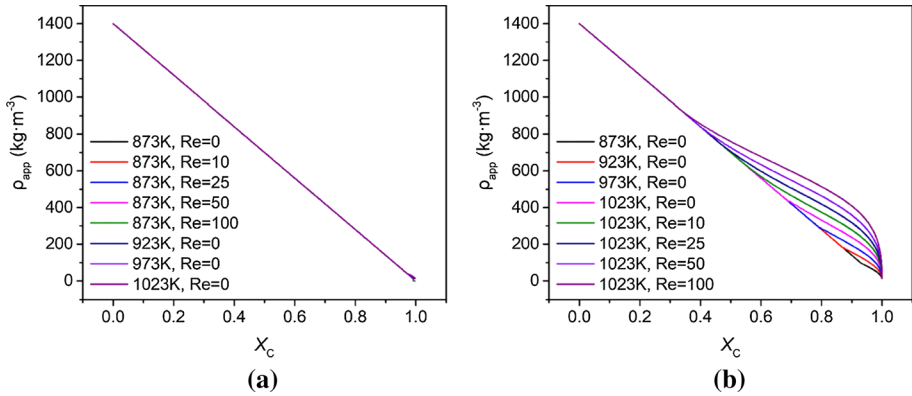


Fig. 6 Particle apparent density evolution with X_c for particles of 0.1 mm (a) and 1 mm (b)

particle radius to reduce earlier. For such situations in zone II regime, the two stages of structure evolution might be treated separately in the model for char particle conversion (Haugen et al. 2014).

3.3 Effectiveness Factor

The effectiveness factor η was introduced to quantify the influence of internal diffusion. It is defined as the ratio of actual particle consumption rate to the particle consumption rate with infinitively fast diffusion by assuming the species concentration is uniform inside the particle and equal to the value at the external surface. Actually, the concept of effectiveness factor has been widely used in char particle conversion simulation in reactors to avoid intensive computational efforts in spatially resolved gradient calculation (Vascellari et al. 2015; Backreedy et al. 2006). Figure 7 shows the effectiveness factor evolution in the particle gasification process. Given the assumption that the porous particle was filled with CO_2 initially, the effectiveness factor was close to 0 at the beginning of the reaction. Subsequently, the effectiveness factor gradually increased to 1 as SCW diffused into the

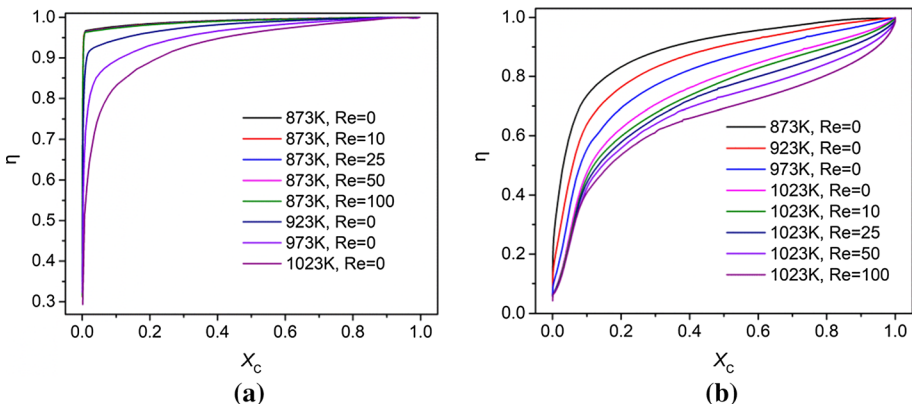


Fig. 7 Effectiveness factor evolution with X_c for particles of 0.1 mm (a) and 1 mm (b)

porous particle and carbon consumption slowed down. For the small particle gasification at 873 K, the effectiveness factor increased immediately to close to 1 after the particle was placed in SCW, indicating that the SCW could rapidly diffuse into the particle to replace the previous CO_2 . Therefore, from the time scale of the whole gasification process, the initial selected species inside the particle had little effect on the overall conversion process. With the increase of temperature, more SCW was consumed in the diffusion process and the concentration gradient became larger, causing a smaller effectiveness factor at the same X_c . Furthermore, the effectiveness factor for the large particle of 1 mm increased significantly more slowly than that for the small particle of 0.1 mm, because SCW was consumed faster and more difficult to diffuse into the large particle. It was also observed that the effectiveness factor decreased with Re for the large particle gasification at 1023 K, which indicated convection contributed more to heat transfer enhancement than to mass transfer enhancement.

3.4 Stefan Flow

The heterogeneous reactions on the particle and pore surface will induce extra Stefan flow which might modify the existing flow field and have impacts on the drag force and particle conversion behavior (Dierich et al. 2018; Zhang et al. 2020; Chen et al. 2020; Jin et al. 2021). The flow fields under typical conditions considering the effect of Stefan flow are displayed in Fig. 8. For particle gasification in quiescent SCW under conditions I and III, Stefan flow from inside and toward outside of the particle can be obviously

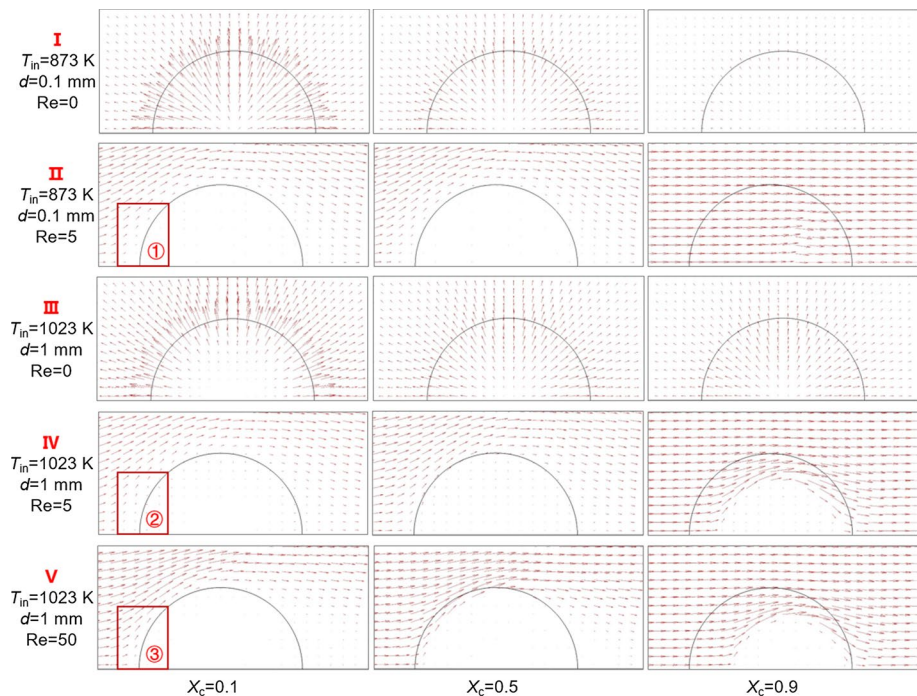


Fig. 8 Vector plots of velocity field at different X_c and under different conditions

observed. The gasification reactions occurred uniformly in the whole particle under the condition I in zone I regime, while the velocity increased radially toward outside due to the superposition of Stefan flow. As the carbon conversion increased, the carbon consumption rate decreased and the Stefan flow weakened accordingly. It was also observed that the main gasification area moved from periphery to center of the particle under condition III in zone II regime. At the X_c of 0.1, strong Stefan flow can be seen near the particle surface, while the flow velocity near the particle center was tiny. As the X_c increased to 0.5 and 0.9, the Stefan flow in the particle outer layer significantly weakened due to the slowing carbon consumption, and the flow became more obvious in the main gasification area near the particle center.

Under convective conditions II, IV and V, the flow resistance inside the particle was large due to the low porosity in the early stage, which inhibited the entrance of ambient SCW. Additionally, the Stefan flow was much weaker than the external flow, so the flow velocity inside the particles was small. For example, the flow velocity inside the particles was 4 orders of magnitude lower than the inflow velocity at the X_c of 0.1 and 0.5 under condition II in zone I regime. As more carbon was consumed, the particle porosity increased and more SCW can permeate into the particle. At the X_c of 0.9, the particle porosity reached 0.93, and the ambient fluid can almost flow through the particle freely. Under conditions IV and V in zone II regime, however, the central porosity was still small even at a high X_c of 0.9, causing the fluid to flow around the irregular unreacted core instead of passing through the entire particle. Besides, the flow field distribution was different under conditions IV and V because of the smaller unreacted core at larger Re. Then, the Stefan flow characteristics under convective conditions were further investigated with the marked flow field areas in Fig. 8 enlarged as shown in Fig. 9. It can be seen clearly in Fig. 9b that the Stefan flow inhibited the penetration of the ambient fluid into the particle and had a significant modification to the hydrodynamic boundary layer. As shown in Fig. 9a, although at the same Re, the Stefan flow was weaker due to smaller particle and slower gasification at 873 K; thus, its influence was insignificant. As shown in Fig. 9c, the Stefan flow intensity was comparable to that in Fig. 9b, but its influence was weakened by strong external convection.

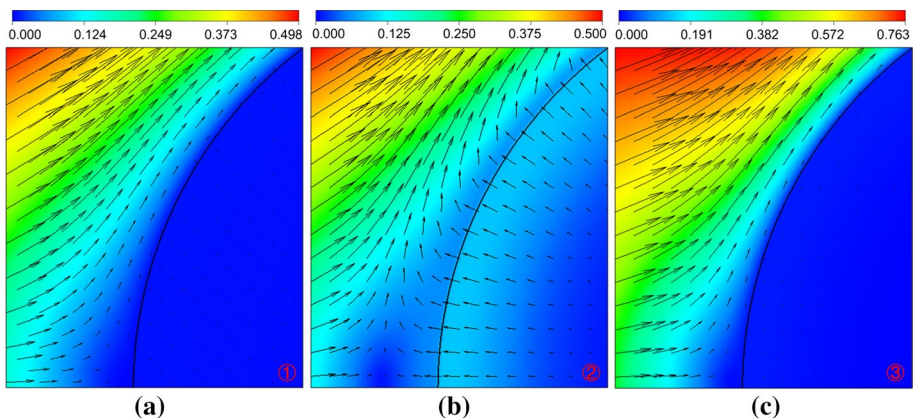


Fig. 9 Local velocity field near the particle surface on the upwind side (the value in the legend represents the ratio of local velocity to inflow velocity)

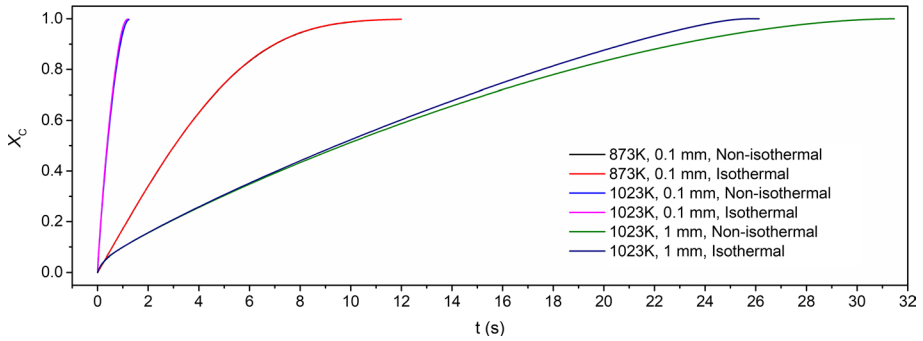


Fig. 10 Carbon conversion plots with time for different cases

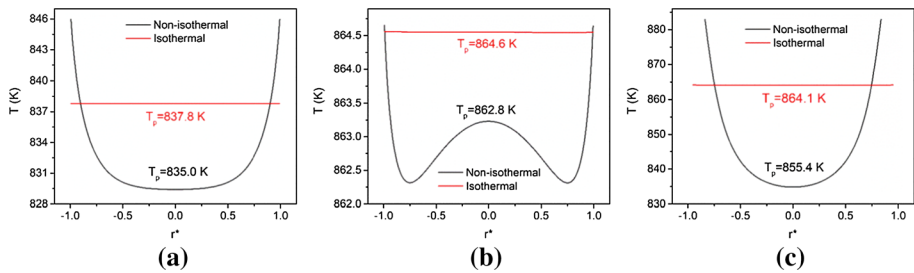


Fig. 11 Temperature profiles at X_c of 0.1 (a), 0.5 (b) and 0.9 (c) inside the particle of 1 mm at 1023 K (T_p is the volume-averaged particle temperature)

3.5 Particle Thermal Conductivity

For general reactor-scale models where each individual particle was tracked (Zhang et al. 2016; Adamczyk et al. 2014) and some highly spatial-resolved particle-scale models (Wittig et al. 2017; Mitchell et al. 2007; Numazawa et al. 2020), the temperature gradient inside the particle was ignored in consideration of the model complexity and computational cost. In this section, the rationality of this assumption in simulation on char gasification in SCW is discussed. The carbon thermal conductivity was assumed to be large enough to obtain uniform temperature distribution inside the particle for comparison, and the effects of temperature and particle size are shown in Fig. 10. The temperature gradient was negligible for the small particle gasification at 873 K because of uniform and slow reactions inside the particle, so the assumption was acceptable. As the temperature increased to 1023 K, the simplification of isothermal particle will overestimate the particle consumption rate. The complete carbon consumption time $t_{0.99}$, defined as the time when X_c reached 0.99, decreased from 1.16 to 1.09 s, by 6.0%. For the large particle gasification at 1023 K, $t_{0.99}$ even decreased from 29.19 to 24.64 s, by 15.6%, because of larger temperature gradient inside the particle. Therefore, the simplification should be used carefully, especially for large particles and at high gasification temperatures.

Figure 11 shows the temperature distribution inside the large particle at 1023 K. The volume-averaged temperature of the isothermal particle was higher than the actual value at any X_c because of higher heat transfer efficiency from ambient fluid to the particle.

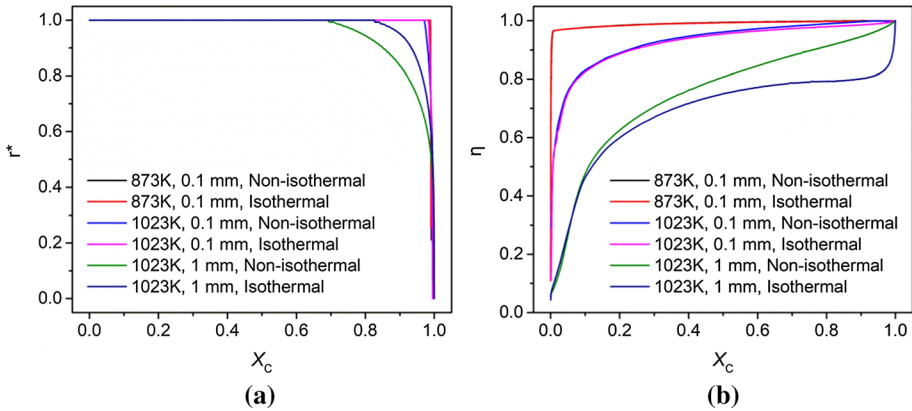


Fig. 12 Evolution of particle radius and effectiveness factor with X_c for different cases

However, the temperature near the particle edge was underestimated because heat transfer to the low-temperature particle center was quick under high thermal conductivity. Moreover, the reactions occurred uniformly inside the particle, delaying the beginning of particle radius reduction, as seen in Fig. 12a. For the isothermal particle, the heterogeneous reactions were more affected by SCW distribution. SCW consumption was faster at the overestimated particle temperature, so smaller effectiveness factor is observed in Fig. 12b.

4 Conclusion

In this work, a CFD-based 2D numerical model was developed for gasification of a single char particle in SCW. The char particle was assumed to be a uniform porous sphere initially, and the particle porosity and specific surface area were allowed to change as char consumption. The coupling processes of flow, heat transfer, species transport and both homogeneous and heterogeneous reactions were considered. The effects of particle size, inflow temperature and inflow velocity were studied based on the model.

For the small particle of 0.1 mm, SCW showed good permeability into the porous char, resulting in a high effectiveness factor in the SCWG process. The structure evolution showed typical characteristic in zone I that the particle radius kept constant and the apparent density changed linearly with carbon conversion, due to relatively uniform reaction inside the particle. The ambient fluid can flow through the particle freely at the carbon conversion of 0.9 at 873 K. For the large particle of 1 mm, the obvious species concentration gradients caused a relatively low effectiveness factor and the particle was consumed non-uniformly. The gasification lay in zone II regime where the particle began to shrink at a certain carbon conversion. The particle shrinkage phenomenon occurred earlier at larger inflow temperature and velocity, so the fluid just flowed around the unreacted core even at a high carbon conversion. When the temperature and particle size increased, the Stefan flow showed more obvious effect on the hydrodynamic boundary layer near the particle surface, especially at low Re , and meanwhile, larger deviation would be caused under the isothermal particle assumption.

Acknowledgements This work was financially supported by the National Natural Science Foundation of China (51922086) and the National Key R&D Program of China (2020YFA0714400).

Declarations

Conflict of interest The authors declare they have no conflict of interest/competing interests.

Ethics approval This work neither was submitted nor is being considered for publication elsewhere.

Consent to participate The authors consent on the participation of this work. The work being carried out was data independent.

Consent for publication The authors consent to the publication of this work.

References

- Adameczyk, W.P., Węcel, G., Klajny, M., Kozotub, P., Klimanek, A., Białecki, R.A.: Modeling of particle transport and combustion phenomena in a large-scale circulating fluidized bed boiler using a hybrid Euler-Lagrange approach. *Particuology* **16**, 29–40 (2014)
- Backreedy, R., Fletcher, L., Ma, L., Pourkashanian, M., Williams, A.: Modelling pulverised coal combustion using a detailed coal combustion model. *Combust. Sci. Technol.* **178**(4), 763–787 (2006)
- Beckmann, A.M., Bibrzycki, J., Mancini, M., Szłęk, A., Weber, R.: Mathematical modeling of reactants' transport and chemistry during oxidation of a millimeter-sized coal-char particle in a hot air stream. *Combust. Flame* **180**, 2–9 (2017)
- Bhatia, S.K., Perlmutter, D.: A random pore model for fluid-solid reactions: I. Isothermal, kinetic control. *AIChE J.* **26**(3), 379–386 (1980)
- Bhunia, S., Sadhukhan, A.K., Gupta, P.: Modelling and experimental studies on oxy-fuel combustion of coarse size coal char. *Fuel Process. Technol.* **158**, 73–84 (2017)
- Chen, T., Ku, X., Lin, J.: CFD simulation of the steam gasification of millimeter-sized char particle using thermally thick treatment. *Combust. Flame* **213**, 63–86 (2020)
- Dierich, F., Richter, A., Nikrityuk, P.: A fixed-grid model to track the interface and porosity of a chemically reacting moving char particle. *Chem. Eng. Sci.* **175**, 296–305 (2018). <https://doi.org/10.1016/j.ces.2017.09.055>
- Ergun, S.: Fluid flow through packed columns. *Chem. Eng. Prog.* **48**, 89–94 (1952)
- Fan, C., Guo, S., Jin, H.: Numerical study on coal gasification in supercritical water fluidized bed and exploration of complete gasification under mild temperature conditions. *Chem. Eng. Sci.* **206**, 134–145 (2019)
- Fan, C., Cao, C., Ge, Z., Chen, Y., Jin, H.: Numerical simulation of a reacting porous char particle in supercritical water with structural evolution. *Appl. Therm. Eng.* **180**, 115864 (2020). <https://doi.org/10.1016/j.applthermaleng.2020.115864>
- Fong, G.H., Jorgensen, S., Singer, S.L.: Pore-resolving simulation of char particle gasification using micro-CT. *Fuel* **224**, 752–763 (2018)
- Guo, L., Jin, H.: Boiling coal in water: Hydrogen production and power generation system with zero net CO₂ emission based on coal and supercritical water gasification. *Int. J. Hydrogen Energy* **38**(29), 12953–12967 (2013). <https://doi.org/10.1016/j.ijhydene.2013.04.089>
- Haugen, N.E.L., Tilghman, M.B., Mitchell, R.E.: The conversion mode of a porous carbon particle during oxidation and gasification. *Combust. Flame* **161**(2), 612–619 (2014)
- Haugen, N.E.L., Mitchell, R.E., Tilghman, M.B.: A comprehensive model for char particle conversion in environments containing O₂ and CO₂. *Combust. Flame* **162**(4), 1455–1463 (2015)
- Jiang, P., Yang, H., Ma, X.: Coal production and consumption analysis, and forecasting of related carbon emission: evidence from China. *Carbon Manag.* **10**(2), 189–208 (2019)
- Jin, H., Fan, C., Wei, W., Zhang, D., Sun, J., Cao, C.: Evolution of pore structure and produced gases of Zhudong coal particle during gasification in supercritical water. *J. Supercrit. Fluids* **136**, 102–109 (2018)
- Jin, H., Wang, Y., Wang, H., Wu, Z., Li, X.: Influence of Stefan flow on the drag coefficient and heat transfer of a spherical particle in a supercritical water cross flow. *Phys. Fluids* **33**(2), 023313 (2021)

- Kaushal, P., Abedi, J., Mahinpey, N.: A comprehensive mathematical model for biomass gasification in a bubbling fluidized bed reactor. *Fuel* **89**(12), 3650–3661 (2010)
- Li, X., Wu, Z., Wang, H., Jin, H.: The effect of particle wake on the heat transfer characteristics between interactive particles in supercritical water. *Chem. Eng. Sci.* **247**, 117030 (2022)
- Mitchell, R.E., Ma, L., Kim, B.: On the burning behavior of pulverized coal chars. *Combust. Flame* **151**(3), 426–436 (2007)
- Numazawa, Y., Saito, Y., Matsushita, Y., Aoki, H.: Large-scale simulation of gasification reaction with mass transfer for metallurgical coke: model development. *Fuel* **266**, 117080 (2020)
- Rabaçal, M., Costa, M., Vascellari, M., Hasse, C., Rieth, M., Kempf, A.M.: A large eddy simulation study on the effect of devolatilization modelling and char combustion mode modelling on the structure of a large-scale, biomass and coal co-fired flame. *J. Combust.* **2018**, 7036425 (2018)
- Ren, Z., Guo, L., Jin, H., Luo, K.: Integration of CFD codes and radiation model for supercritical water gasification of coal in fluidized bed reactor. In: *International Heat Transfer Conference Digital Library 2018*. Begel House Inc.
- Sadhukhan, A.K., Gupta, P., Kumar Saha, R.: Modeling and experimental studies on combustion characteristics of porous coal char: Volume reaction model. *Int. J. Chem. Kinet.* **42**(5), 299–315 (2010a)
- Sadhukhan, A.K., Gupta, P., Saha, R.K.: Modelling of combustion characteristics of high ash coal char particles at high pressure: Shrinking reactive core model. *Fuel* **89**(1), 162–169 (2010b)
- Senneca, O., Salatino, P.: Loss of gasification reactivity toward O₂ and CO₂ upon heat treatment of carbons. *Proc. Combust. Inst.* **29**(1), 485–493 (2002)
- Singer, S.L., Ghoniem, A.F.: Comprehensive gasification modeling of char particles with multi-modal pore structures. *Combust. Flame* **160**(1), 120–137 (2013)
- Su, X., Guo, L., Jin, H.: Mathematical Modeling for Coal Gasification Kinetics in Supercritical Water. *Energy Fuels* **30**(11), 9028–9035 (2016)
- Szekely, J.: *Gas-Solid Reactions*. Elsevier, New York (2012)
- Tufano, G.L., Stein, O.T., Kronenburg, A., Gentile, G., Stagni, A., Frassoldati, A., Faravelli, T., Kempf, A.M., Vascellari, M., Hasse, C.: Fully-resolved simulations of coal particle combustion using a detailed multi-step approach for heterogeneous kinetics. *Fuel* **240**, 75–83 (2019). <https://doi.org/10.1016/j.fuel.2018.11.139>
- Vascellari, M., Roberts, D.G., Harris, D.J., Hasse, C.: From laboratory-scale experiments to industrial-scale CFD simulations of entrained flow coal gasification. *Fuel* **152**, 58–73 (2015)
- Wagner, W., Cooper, J.R., Dittmann, A., Kijima, J., Kretzschmar, H.-J., Kruse, A., Mareš, R., Oguchi, K., Sato, H., Stöcker, I., Šifner, O., Takaishi, Y., Tanishita, I., Trübenbach, J., Willkommen, T.: The IAPWS industrial formulation 1997 for the thermodynamic properties of water and steam. *J. Eng. Gas Turbines Power* **122**(1), 150–184 (2000). <https://doi.org/10.1115/1.483186>
- Wittig, K., Nikrityuk, P.A., Schulze, S., Richter, A.: Three-dimensional modeling of porosity development during the gasification of a char particle. *AIChE J.* **63**(5), 1638–1647 (2017)
- Yuan, J., Na, C., Lei, Q., Xiong, M., Guo, J., Hu, Z.: Coal use for power generation in China. *Resour. Conserv. Recycl.* **129**, 443–453 (2018)
- Zhang, Z., Li, Z., Cai, N.: Reduced-order model of char burning for CFD modeling. *Combust. Flame* **165**, 83–96 (2016)
- Zhang, H., Luo, K., Haugen, N.E.L., Mao, C., Fan, J.: Drag force for a burning particle. *Combust. Flame* **217**, 188–199 (2020)
- Zhao, X., Jin, H.: Correlation for diffusion coefficients of H₂, CH₄, CO, O₂ and CO₂ in supercritical water from molecular dynamics simulation. *Appl. Therm. Eng.* **171**, 114941 (2020)
- Zhao, S., Wang, C., Bai, B., Jin, H., Wei, W.: Study on the polystyrene plastic degradation in supercritical water/CO₂ mixed environment and carbon fixation of polystyrene plastic in CO₂ environment. *J. Hazard. Mater.* **421**, 126763 (2021)